Available online at www.sciencedirect.com
SCIENCE DIRECT
Journal of Solid State Chemistry 179 (2006) 2645–2655
JOURNAL OF SOLID STATE CHEMISTRY
www.elsevier.com/locate/jssc

$Ba_3Fe_2WO_{9-\delta}$: Effect of oxygen non-stoichiometry on structural and magnetic properties

S.A. Ivanov[a,*], S.-G. Eriksson[b], R. Tellgren[c], H. Rundlof[c], P. Nordblad[d], J. Eriksen[e]

[a]*Department of Inorganic Materials, Karpov' Institute of Physical Chemistry, Vorontsovo pole,10 105064 Moscow K-64, Russia*
[b]*Environmental Inorganic Chemistry, Chalmers University of Technology, SE-412 96, Gothenburg, Sweden*
[c]*Department of Materials Chemistry, The Ångström Laboratory, Box 538, University of Uppsala, SE-751 21, Uppsala, Sweden*
[d]*Department of Engineering Sciences, University of Uppsala, Uppsala, Sweden*
[e]*NFL Studsvik, University of Uppsala, Sweden*

Received 12 December 2005; received in revised form 21 March 2006; accepted 8 April 2006
Available online 10 May 2006

Abstract

The magnetic and structural properties of oxygen-deficient perovskites with composition $Ba_3Fe_2WO_{9-\delta}$ (BFWO) have been systematically studied for two different oxygen contents corresponding to $\delta = 0.00$ and 0.55 in the chemical formula in order to determine and correlate their chemical composition, structural and magnetic properties. The evolution of nuclear and magnetic structures with temperature has been investigated by neutron powder diffraction. It was shown that at room temperature the stoichiometric compound ($\delta = 0.00$) adopts a hexagonal 6H-perovskite structure (space group $P6_3/mmc$). This phase, when heated at high temperature under a stream of Ar gas, transforms to an oxygen-deficient phase $\delta = 0.55$), which is an ordered cubic perovskite structure (space group $Fm-3m$). The crystallographic and magnetic properties of the obtained phases are compared, and it is clear that the magnetic properties are significantly affected by oxygen non-stoichiometry. These changes of magnetic properties for such a slight decrease in oxygen content are interpreted as a result of structural transformations. Together with the experimental results based on neutron powder diffraction data a discussion of some aspects of the structural transformation ($P6_3/mmc \rightarrow Fm-3m$) is presented.

Keywords: A. Ceramics; C. Neutron scattering; D. Crystal structure; D. Magnetic structure

1. Introduction

Magnetoelectric materials, that simultaneously show an electric and magnetic order, are currently gaining more and more attention because of their novel phenomena and possible applications in new modern devices [1–4]. Generally, ferroelectricity is not compatible with ferromagnetism due to the structural restrictions and therefore chances to find new magnetoelectric materials are very limited [5]. Ferroelectricity appears only in a non-centrosymmetric structure in contrast to a magnetic ion preferring a centrosymmetric surrounding. Hence, magnetoelectrics are very rare materials and until now only a few compounds have been reported to exhibit both ferroelectric and ferromagnetic properties within the same phase [6]. Most of the perovskite magnetoelectrics reported so far are antiferromagnets without spontaneous magnetization, in which a conspicuous response to the application of magnetic fields cannot be expected. Search and design of new magnetoelectric perovskite materials with preselected functionalities began in the 1950s with the substitution of diamagnetic cations by paramagnetic ones in the perovskite B-sublattice [7]. At the same time it was found that the presence of diamagnetic ions with inert gas electron configuration (W^{+6} for example) would be beneficial in stabilizing ferroelectric properties in such complex perovskite structured metal oxides [8]. When the B-sites in the perovskite oxide are partly occupied by transition metal cations, the magnetic properties are strongly influenced by the ordering of the B-site ions. Known ferromagnetic

*Corresponding author.
E-mail addresses: ivan@cc.nifhi.ac.ru (S.A. Ivanov), stene@chalmers.se (S.-G. Eriksson), rte@mkem.uu.se (R. Tellgren).

0022-4596/$ - see front matter © 2006 Published by Elsevier Inc.
doi:10.1016/j.jssc.2006.04.050

ferroelectrics have unfortunately been studied with different degrees of thoroughness, and technical applications of these materials are severely limited [9,10]. In many cases only data on their temperatures of ferroelectric and magnetic phase transitions T_{CE} and T_{CM} are available. Only sparse data is available on their crystal and magnetic structures.

Much of our recent research has been focussed on the dielectric and magnetic properties of iron-based double perovskites $A_3Fe_2WO_9$ (A = Ba, Pb, Sr, Ca) [11–13], which have a great interest in many applied and fundamental areas of solid state chemistry, physics and advanced materials. These oxides exhibit rather unusual magnetic and dielectric properties leading to a number of original materials. Such materials were initially synthesized and investigated in the mid-1960s [8,14,15] and then forgotten for a number of years. These compounds have, however, regained much interest, which arises from the prospects of finding half-metallic oxides showing high Curie temperatures.

In this paper we turn our attention to the structural and magnetoelectric properties of perovskites $Ba_3Fe_2WO_{9-\delta}$ (BFWO). Although the dielectric, magnetic and structural characteristics of stoichiometric BFWO already has been studied [13,16,17], their defect chemistry is complex and poorly understood. In addition, very little is known about the possible polymorphs, which exist for different oxygen-deficient compositions. The details of the nuclear and magnetic structure of non-stoichiometric BFWO as a function of temperature have not yet been described either. Previously it has been shown [18] that this stoichiometric BFWO compound has a hexagonal structure (space group $P6_3/mmc$) at room temperature. Heated at 1350 °C under a stream of helium BFWO form an oxygen-deficient cubic perovskite phase (space group $Fm-3m$). However, the tested samples were not pure and some amount of second phase $BaWO_4$ was found in addition to the main hexagonal phase.

Complex metal oxide perovskites are characterized by mixed-valent transition metal cation (Fe in our case) and may support a large oxygen non-stoichiometry. The magnetic properties of these compounds are thought to arise from a super-exchange mechanism involving 3*d*-electrons of Fe cations and oxygen *p*-orbitals. Thus oxygen plays a very important role in magnetic ordering of these compounds and modification of anion composition is effective for controlling the crystal structure and fundamental physical properties of these perovskites. In order to study the effect of oxygen non-stoichiometry on the structural and magnetic properties of BFWO, we have undertaken a detailed study of this compound. Accurate neutron powder diffraction (NPD) data may help to determine the key factors responsible for the structural transformations and magnetic interactions in this material. The advantage of neutrons instead of X-rays for structural studies of complex metal oxides (containing light anions in the presence of heavy cations) is well known. From X-ray experiments it is quite difficult to obtain precise qualitative information about the anion sublattice, which gives only a minor contribution to the X-ray diffraction pattern.

In this work, we report the results of a NPD study and magnetic measurements of non-stoichiometric BFWO in the temperature range 10–700 K. The objective of our research is to relate the chemical composition and structural changes, as determined from NPD data, to the observed magnetic properties.

2. Experimental

A high-quality stoichiometric polycrystalline sample of hexagonal BFWO was prepared by a conventional solid-state sintering procedure, which was described in [13]. As starting materials $BaCO_3$, Fe_2O_3 and WO_3 were used. Appropriate amounts of starting materials, with respect to metal ratio, were mixed and thoroughly milled in an agate mortar. The mixed powder was placed in an alumina crucible and calcined at 950 °C for 15 h in an O_2 environment. The sample was pressed into a pellet and then reacted at 1100 °C for 2 days and for another 2 days at 1300 °C in an O_2 environment with several intermediate grindings, and with new pellets made after each grinding step. The samples were characterized by X-ray powder diffraction (Guinier film data, Cu$K\alpha$1-radiation) for phase identification and to check phase purity. The prepared sample was pure single phase (without any amount of $BaWO_4$) and did not exhibit any superstructure reflections due to cation ordering of Fe and W on the B-sites in the double-perovskite structure. Electron probe microanalysis showed that the studied sample had a cation composition of $Ba_{3.01(1)}Fe_{1.99(1)}W_{1.01(1)}O_9$, which was close to the expected ratio.

The oxygen-deficient cubic BFWO sample was prepared from the hexagonal compound by sintering at high temperature in a strongly reducing atmosphere (5%H_2 in Ar). The temperature was gradually increased as follows: 12 h at 650 °C, 12 h at 700 °C, 24 h at 800 °C, 12 h at 850 °C and finally 12 h at 900 °C. During this procedure the initial hexagonal phase first lost some oxygen but retained the current symmetry with the lattice parameters slightly changed. Additional heating signify that a mixture of two coexisting phases (cubic and hexagonal) appeared. The intensity of the new reflections from the cubic phase increased progressively, whereas the peaks from hexagonal phase became weaker and weaker and finally disappeared after several hours of firing as describe above. The inductively coupled plasma atomic emission spectroscopy (ICP-AES) performed with an ARL Fisons 3410 spectrometer showed that the obtained sample had practically the same cation composition, namely $Ba_{2.99(1)}Fe_{2.00(1)}W_{1.01(1)}O_{9-\delta}$, as for initial hexagonal phase. The non-stoichiometry δ of the sample was determined by chemical titration. The oxygen deficiency parameter ($9-\delta$) for the cubic BFWO sample was estimated to 8.49(2).

Phase purity of this sample was identified by X-ray diffractometry, using a Siemens D-5000 diffractometer (Cu$K\alpha$ radiation) equipped with a nickel filter.

Medium-resolution NPD data were collected at the Swedish Research reactor R2 in Studsvik at the Huber two-circle diffractometer equipped with an array of 35 ^{3}He detectors. The intensity from each detector was statistically analysed and summed. The monochromator system used consisted of two copper crystals with (220) lattice planes in a parallel arrangement. The wavelength was 1.470(1) Å and the neutron flux at the sample position approximately 10^6 neutrons cm^{-2} s^{-1}. Diffraction patterns were registered at temperatures 10, 100, 200 and 300 K. The powder sample of BFWO (approximately 3 g) was loaded into a thin-walled vanadium container and mounted in a cryostat. Absorption effects were later corrected for in the Rietveld refinements using the experimentally determined value $\mu R = 0.1119$ cm^{-1}. The step-scan covered a 2θ-range 4.00° to 139.92° with a step-length 0.08°, and each data collection taking approximately 16 h. The diffraction data were analysed by the Rietveld method using the FULLPROF software [19]. Scattering lengths and form factors for Ba, Fe, W and O were taken from the library of the program ($b_{Ba} = 5.07$, $b_{Fe} = 9.45$, $b_W = 4.86$, $b_O = 5.803$ fm). The diffraction peaks were described by a pseudo-Voigt function where a Lorentzian contribution to the Gaussian peak shape is refined. Peak asymmetry correction was made for angles below 35° in 2θ. The background was described by a six-parameter polynomial. During the refinements the two octahedrally coordinated metal cations (Fe and W) were allowed to vary their proportions on the two possible metal sites. Each structural model was refined to convergence. The best result was chosen on the basis of agreement factors and stability of the refinement.

Magnetic measurements were made in a Quantum Design SQUID magnetometer at different magnetic fields in the temperature range 5–600 K. Zero field cooled measurements (ZFC) were performed by cooling the samples to 10 K, applying the field, and measuring the magnetization as the samples were heated.

3. Results

Fig. 1a shows the temperature dependence of magnetization for prepared non-stoichiometric $Ba_3Fe_2WO_{8.45}$ sample. The magnetization was measured in an applied field of 100 Oe after cooling in ZFC and on cooling in the same field (FC). Similar measurements in an applied field of 1000 Oe are shown in Fig. 1b for the stoichiometric sample $Ba_3Fe_2WO_9$. The $Ba_3Fe_2WO_{8.45}$ sample shows a paramagnetic to ferrimagnetic transition around 340 K. The magnetization versus magnetic field curves at 10 K are plotted in Fig. 2 (two upper curves). For $H = 10$ KOe, a maximum magnetization value close to $0.8\,\mu_B$/Fe is observed, although a full saturation is not reached. The magnetic behaviour of the stoichiometric hexagonal

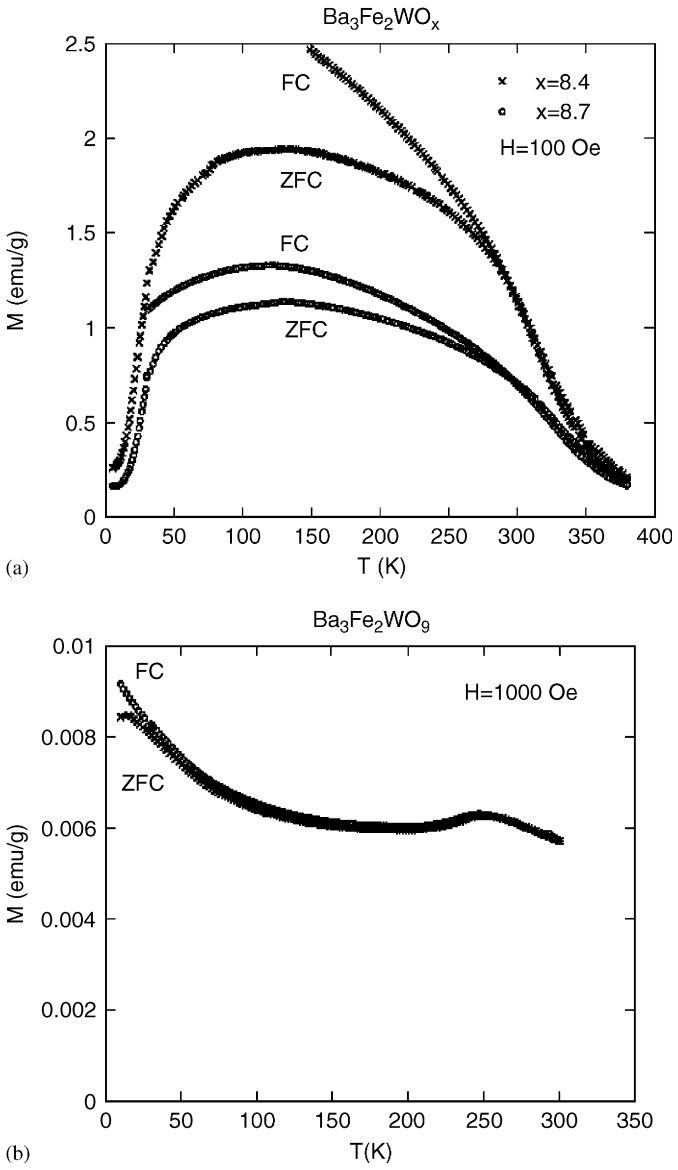

Fig. 1. Temperature dependence of the magnetization for $Ba_3Fe_2WO_X$ ($x = 8.45$ and 8.72) samples in 100 Oe applied field (a) and $Ba_3Fe_2WO_9$ sample in 1000 Oe applied field (b).

compound is markedly different (see Figs. 1b and 2): (1) a clear maximum on M vs. T plot is observed near 250 K, indicating a long-range antiferromagnetic ordering; (2) The variation of M vs. H is practically linear; (3) The magnetization value obtained with the maximum field (10 KOe) is significantly less (about 0.006 μ_B/Fe) compared with $Ba_3Fe_2WO_{8.45}$ sample.

The quality of the sample and its crystallographic structure has been studied firstly by means of XRD at room temperature. Rietveld analysis of the registered spectra revealed that the tested compound is essentially single phase. XRD patterns of oxygen-deficient BFWO could be readily identified as representing a perovskite-related phase and the room temperature diffractogram could be indexed on the basis of a cubic unit cell. Similar results have been reported earlier [18] where it was claimed

that 6% oxygen vacancies in BFWO hardly modifies the symmetry and the magnetic behaviour.

The systematic absences observed in both the XRD and NPD patterns are compatible with the space group $Fm-3m$. This space group allows two crystallographically distinct octahedral sites in the double perovskite structure, thus permitting an ordered arrangement between Fe and W cations. NPD measurements were performed between 10 and 700 K in order to check whether or not any phase transition occurred in BFWO, and in order to determine the temperature evolution of nuclear and magnetic structures. The diffraction profiles are shown in Fig. 3. The crystal structure at 10 K is the same as that at 700 K. A comparison of the NPD patterns shows that some magnetic scattering appears near room temperature and exists down 10 K. The positions of the magnetic reflections are in accordance with those of the nuclear ones. Using the Rietveld method the nuclear and magnetic structures were determined (see Fig. 4).

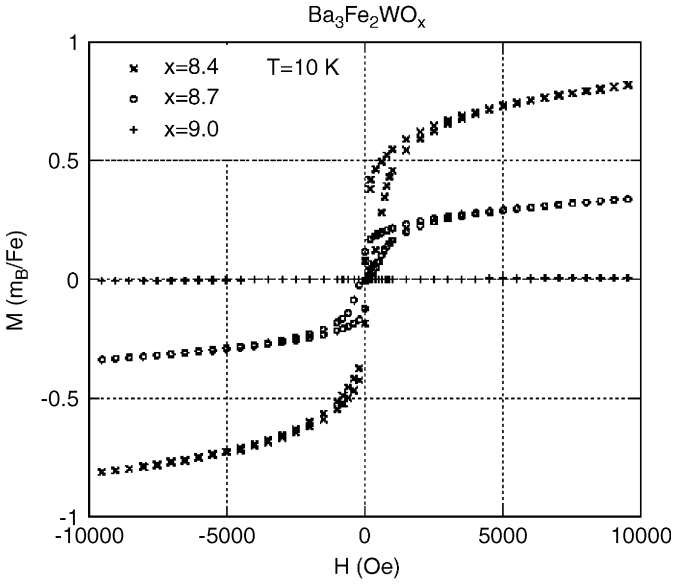

Fig. 2. Magnetization-field (M–H) loops ($T = 10$ K) for different $Ba_3Fe_2WO_X$ samples ($x = 8.45$, 8.72 and 9.0).

Initially it was assumed that there was no magnetic contribution to the scattering in the room temperature data. Different structural models based on partial ordering between Fe and W cations in the B-sublattice (4a and 4b sites) were tested. BFWO can be represented by the general formula:

$$\underset{(8c)}{Ba_8}\,[\underset{(4a)}{Fe_{4-\lambda}W_{\lambda}}]\,[\underset{(4b)}{Fe_{4/3+\lambda}W_{8/3-\lambda}}]\,\underset{(24e)}{O_{24-x}}\,.$$

Here λ reflects the order between Fe^{3+} and W^{6+} cations.

Using the Rietveld refinements of NPD data at 700 K (paramagnetic phase) the Fe and W distribution over the 4a and 4b sites was refined within the constraints, that the sites remained fully occupied and that the overall Fe:W ratio remained at 2:1. The refinement yielded the parameter $\lambda = 0.00(2)$. No cation disorder was detected and the cation composition was very close to the ideal ratio. Refinements of the site occupancy factors of the oxygen atoms did reveal significant changes from full occupancy. The oxygen deficiency δ was estimated as 0.55(3). The final Fourier difference synthesis calculation showed no significant maxima.

The structure of oxygen-deficient cubic BFWO is illustrated in Fig. 5(a) where two crystallographically distinct octahedral sites create an ordered arrangement between Fe and W cations. Only Fe is observed at (4a) the positions, whereas (4b) sites are occupied by 33% Fe and 67% W. Fig. 5b shows for comparison a view of the crystal structure of hexagonal BFWO. The atomic coordinates and other relevant parameters are collected in Table 1. Selected bond lengths and angles are listed in Table 2.

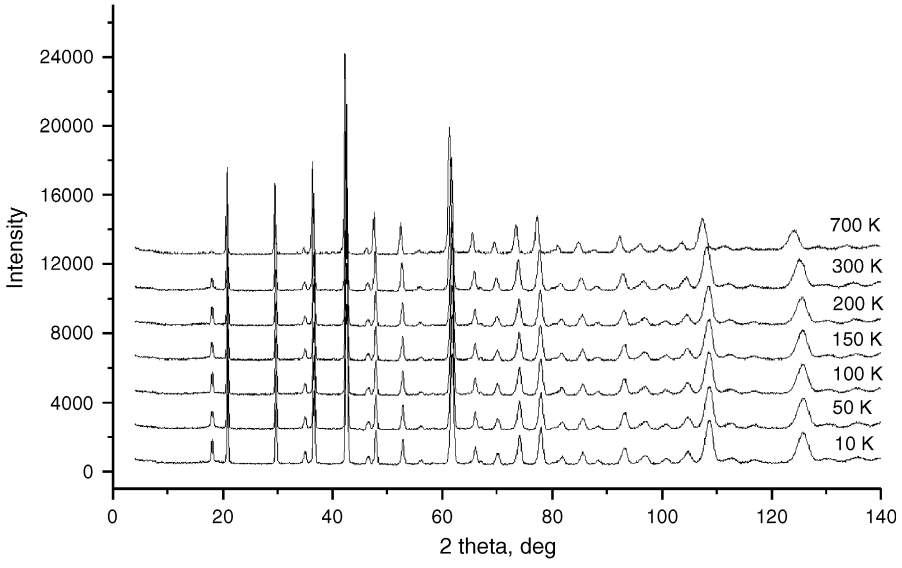

Fig. 3. Temperature evolution of NPD patterns of $Ba_3Fe_2WO_{8.45}$.

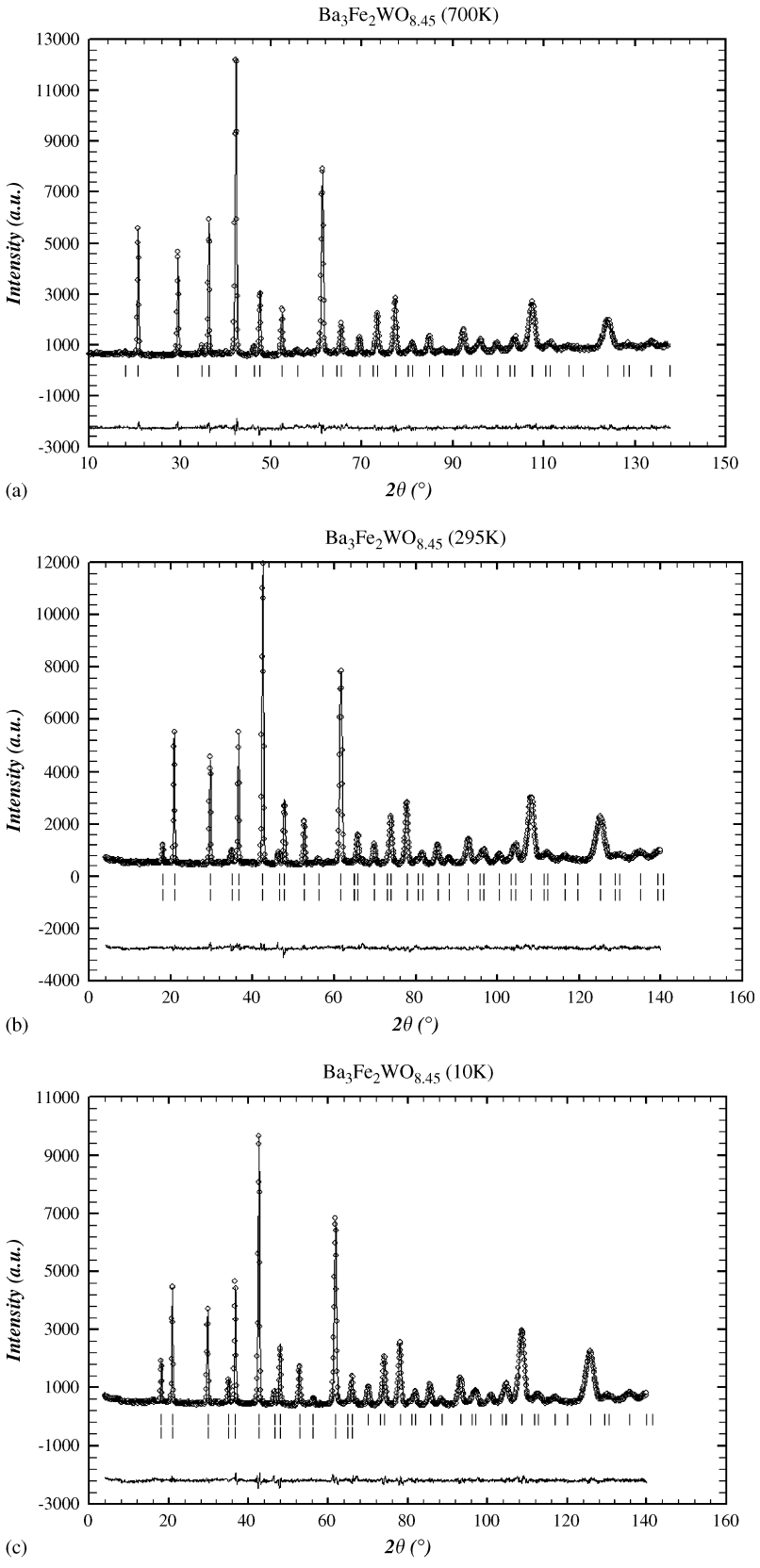

Fig. 4. The observed, calculated, and difference plots for the fit to NPD patterns of $Ba_3Fe_2WO_{8.45}$ after Rietveld refinement of the nuclear and magnetic structure at different temperatures: 700 K (a), 300 K (b) and 10 K(c).

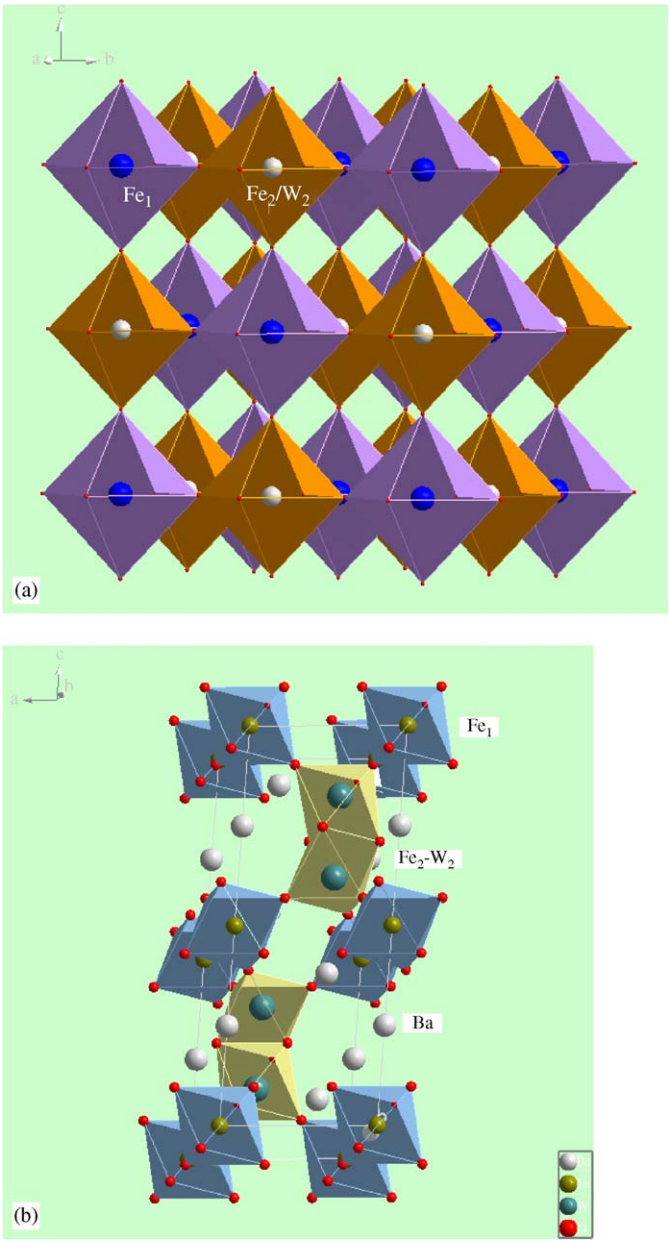

Fig. 5. (a) The ordered cubic perovskite structure of $Ba_3Fe_2WO_{8.45}$ is shown. (b) The crystal structure of fully oxygenated hexagonal 6H-perovskite structured BFWO is shown.

Oxygen anions are located at (x, 0, 0) positions with $x = \frac{1}{4}$ for an ideal $Fm-3m$ cubic structure. Its deviation from $\frac{1}{4}$ determines the difference between the sizes of two B-cation sublattices, which can be observed in Table 2. The Fe_1-octahedron is enlarged compared to the Fe_2/W_2 ones. The sum of Shannon's ionic radii [20] for Fe^{3+}, Fe^{2+} and oxygen gives an average Fe^{3+}–O distance of 2.045 and 2.18 Å for Fe^{2+}–O distance for a 6 coordinated high spin state. In our case the Fe_1–O distance is intermediate between those for Fe^{2+}–O and Fe^{3+}–O and some part of Fe (almost 40%) in this kind of octahedra is supposed to have an oxidation state of 2+. The mean distances of Fe_2/W_2–O are comparable with the distance calculated from the ionic radii.

There is no evidence of any major change in the crystal structure between 10 and 700 K.

The temperature evolution of NPD patterns from 700 to 10 K (see Fig. 3) shows that there is some magnetic contribution to the scattering at low angles, mainly seen on the (111) reflection. Preliminary attempts were made to refine the NPD patterns at all temperatures using a model assumed in accordance with space group $Fm-3m$. These calculations resulted in unacceptably high R-factors. At low 2θ-angles significantly higher observed than calculated intensities were found. Extra intensity was found on the (111) Bragg peaks. The agreement between the observed and calculated intensities did not improve due to shifting of atoms from their ideal positions. The higher-angle data covering $70^\circ < 2\theta < 139.92^\circ$ were refined using the same model and resulted in satisfactory R-factors. It also gave quite reasonable structural parameters, including the isotropic temperature factors. These results indicate that the extra intensities on the low-angle reflections is most likely due to ferrimagnetic ordering of the iron cations. The additional contribution to the scattering was found to disappear above a room temperature that is in full agreement with the results of magnetic measurements.

In order to verify that the observed extra intensities indeed were magnetic to its origin X-ray diffraction measurements were carried out. The variable parameter for the refinement of the magnetic structure was the magnitude of the magnetic moment. The crystal structure of BFWO in the whole temperature interval investigated is cubic (space group $Fm-3m$), and all the magnetic peaks can be indexed within the crystallographic unit cell. Thus the magnetic structure was modeled as an ferrimagnetic arrangement of Fe spins with alternating direction at (4a) and (4b) sites (see Fig. 6). Due to the cubic symmetry, it was impossible to determine the spin direction from powder data.

The perfect magnetic coupling between two different Fe^{3+} spins at (4a) and (4b) positions would give a net magnetization of $5(1-1/3) = 3.33\,\mu_B$. One should have in mind that the 4a site also contains Fe^{2+}. However, when assigning part of the iron as Fe^{2+}, and refining the magnetic structure no improvement was indicated. The magnetization observed in our experiment at 10 K is smaller than the predicted value. The difference may be connected with non-ideal super-exchange interactions through Fe_{4a}–O–Fe_{4b}–O–Fe_{4a} probably arising from an oxygen non-stoichiometry. At the same time, near 40% of Fe in (4a) position have a valence state 2+ ($s = 2$) decreasing the contribution in total magnetization from this site from 5 to 4.6 μ_B (60% Fe^{3+}(5 μ_B) +40% Fe^{2+} (4 μ_B)). As a result, the magnetic interactions are obviously weakened by replacement of Fe^{3+}($s = 5/2$) with Fe^{2+}($s = 2$). The thermal variation of the magnitude of the ordered magnetic moment for different Fe sublattices is displayed in Fig. 7.

Table 1
Structural parameters for $Ba_3Fe_2WO_{8.45}$ at different temperatures

Atom	Position	x	y	z	B/Å^2	n
Ba	(8c)	1/4	1/4	1/4	1.26(4)	1.0
Fe1	(4a)	0	0	0	0.81(5)	1.0
Fe2/W2	(4b)	1/2	1/2	1/2	0.74(5)	0.33/0.67
O	(24e)	0.2587(4)	0	0	1.49(7)	0.94(1)
$T = 700$ K, $a = 8.1540(3)$ Å, $V = 542.15(1)$ Å^3.						
$R_p = 3.66$, $R_{wp} = 4.81$, $R_B = 3.53$, $\chi^2 = 2.29$.						

Atom	Position	x	y	z	B/Å^2	n	$m(\mu_B)$
Ba	(8c)	1/4	1/4	1/4	0.56(4)	1.0	
Fe1	(4a)	0	0	0	0.64(5)	1.0	2.1(1)
Fe2/W2	(4b)	1/2	1/2	1/2	0.57(5)	0.33/0.67	−1.4(2)
O	(24e)	0.2582(4)	0	0	0.84(7)	0.94(1)	
$T = 295$ K, $a = 8.1123(3)$ Å, $V = 533.85(1)$ Å^3.							
$R_p = 3.71$, $R_{wp} = 4.86$, $R_B = 3.64$, $R_{mag} = 6.47$, $\chi^2 = 2.32$.							
Ba	(8c)	1/4	1/4	1/4	0.49(4)	1.0	
Fe1	(4a)	0	0	0	0.56(5)	1.0	2.7(1)
Fe2/W2	(4b)	1/2	1/2	1/2	0.51(5)	0.33/0.67	−1.6(2)
O	(24e)	0.2584(4)	0	0	0.61(7)	0.94(1)	
$T = 200$ K, $a = 8.0998(3)$ Å, $V = 531.40(1)$ Å^3.							
$R_p = 4.01$, $R_{wp} = 5.02$, $R_B = 3.21$, $R_{mag} = 6.24$, $\chi^2 = 2.41$.							
Ba	(8c)	1/4	1/4	1/4	0.46(4)	1.0	
Fe1	(4a)	0	0	0	0.50(5)	1.0	3.0(1)
Fe2/W2	(4b)	1/2	1/2	1/2	0.44(5)	0.33/0.67	−1.8(2)
O	(24e)	0.2586(4)	0	0	0.53(7)	0.94(1)	
$T = 100$ K, $a = 8.0932(3)$ Å, $V = 530.11(1)$ Å^3.							
$R_p = 4.12$, $R_{wp} = 5.09$, $R_B = 3.21$, $R_{mag} = 6.58$, $\chi^2 = 2.49$.							
Ba	(8c)	1/4	1/4	1/4	0.42(4)	1.0	
Fe1	(4a)	0	0	0	0.46(5)	1.0	3.1(1)
Fe2/W2	(4b)	1/2	1/2	1/2	0.40(5)	0.33/0.67	−1.9(2)
O	(24e)	0.2589(4)	0	0	0.49(7)	0.94(1)	
$T = 50$ K, $a = 8.0912(3)$ Å, $V = 529.70(1)$ Å^3.							
$R_p = 4.03$, $R_{wp} = 4.93$, $R_B = 2.83$, $R_{mag} = 6.29$, $\chi^2 = 2.46$.							
Ba	(8c)	1/4	1/4	1/4	0.41(4)	1.0	
Fe1	(4a)	0	0	0	0.45(5)	1.0	3.2(1)
Fe2/W2	(4b)	1/2	1/2	1/2	0.42(5)	0.33/0.67	−2.0(2)
O	(24e)	0.2587(4)	0	0	0.47(7)	0.94(1)	
$T = 10$ K, $a = 8.0906(3)$ Å, $V = 529.59(1)$ Å^3							
$R_p = 4.12$, $R_{wp} = 5.17$, $R_B = 2.83$, $R_{mag} = 6.38$, $\chi^2 = 2.51$							

Space group $Fm-3m$ (225).

Table 2
Selected interatomic distances (Å) and angles (°) for $Ba_3Fe_2WO_{8.45}$ at the different temperatures

Bond	700 K	295 K	200 K	100 K	50 K	10 K
Ba–O	2.884(3)	2.869(2)	2.865(2)	2.862(2)	2.862(2)	2.861(2)
Fe_1–O	2.100(3)	2.098(2)	2.095(2)	2.095(2)	2.093(3)	2.093(2)
Fe_2/W_2–O	1.997(3)	1.959(2)	1.957(2)	1.951(2)	1.951(3)	1.952(2)

4. Discussion

The refined atomic coordinates and bond distances for BFWO (see Tables 1 and 2) confirm the basic structural features of the proposed cubic structure. In order to get some insight into the cation distribution, we carried out bond–valence sum calculations according to Brown's model [21], which gives a relationship between the formal

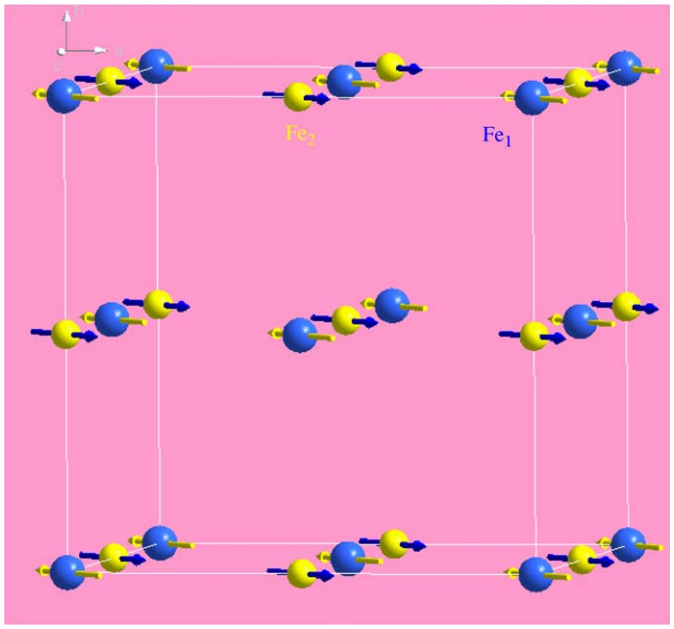

Fig. 6. The magnetic structure of $Ba_3Fe_2WO_{8.45}$. Diamagnetic ions are omitted.

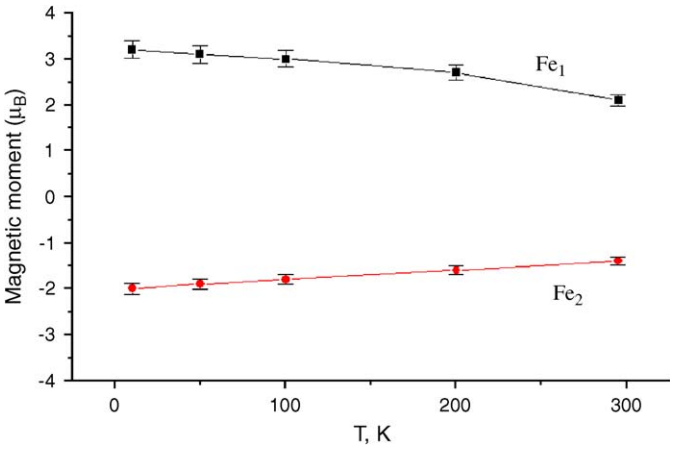

Fig. 7. Temperature dependence of magnetic moment for different Fe sublattices refined from NPD patterns.

valence of a bond and the corresponding bond lengths. In non-distorted structures, the bond–valence sum rule states that the valence of the cation (V_i) is equal to the sum of the bond valences (v_{ij}) around this cation. Any discrepancy from this rule may be a measure of the existing distortion in the bonds and indicates the presence of a covalent contribution to the bonds. From individual cation–anion distances the valences of cations were calculated. The Fe(1) and Fe(2) cations exhibit the valences +2.27(1) and +3.25(1), respectively. On the other hand the valence of the W cation is +5.06(1).

The unit cell volume increases with increasing non-stoichiometry δ for a given cation composition. An interpretation of this trend is straightforward: an increase in oxygen deficiency δ causes the concentration of Fe^{2+} also to increase by 2δ Because of the larger size of Fe^{2+} in comparison with Fe^{3+} the unit cell expands. In addition, the formation of vacant oxygen positions leads to a change of the coordination environment of Fe: a fraction of the Fe-octahedra are transformed into Fe^{2+}–O polyhedra with quadratic pyramidal Fe coordination. The repulsion between two Fe^{2+} in the vicinity of an oxygen vacancy (basal planes of the FeO_5 pyramid face each other) as well as between neighbouring Ba cations increases the size of the unit cell. A similar expansion of the unit cell with increasing non-stoichiometry has also been reported for other oxygen-deficient perovskites [22].

In order to understand the real conditions and simple ways for realization of the hexagonal–cubic phase transformation, the hexagonal polytype of BFWO is presented schematically in Fig. 8b showing $(Fe/W)O_6$ octahedra stacked along the [0001] direction. This structure is built up to of six close-packed layers of BaO_3 appearing under the (*cch*)(*cch*) stacking sequence where *c* stands for cubic and *h* for hexagonal; the *h* layer is a mirror plane. The ratio of face- to apex-sharing linkages in a hexagonal structure is dependent on the size of the A-cation (or the tolerance factor). The average Fe oxidation state also influences the tolerance factor via an influence on the average Fe–O bond length. Thus the ratio of apex- to face-sharing linkages, or more specifically cubic to hexagonally stacked layers, may be controlled by oxygen stoichiometry. The axial ratio c/a at 300 K for the hexagonal phase BFWO was calculated to 2.448, which is very close to the theoretical value of 2.45 expected for the ''undistorted'' hexagonal 6H-type structure.

If some oxygen is removed from the initial hexagonal layer, the face-sharing will be disrupted and two distorted Fe^{2+} trigonal bipyramides sharing an edge. This configuration is highly improbable. The hexagonal structure remains stable until a number of missing oxygens approach a critical value, at which point a sluggish structural transformation to a cubic perovskite may occur. This kind of transformation can be carried out by a ''shear'' action taking place parallel to (110) (for more details consult Ref. [23]).

As shown in Fig. 8b the 6H hexagonal structure can be considered as a regularly twinned cubic perovskite in which the twin composition plane is every third BaO_3 layer parallel to the (111) cubic planes [24]. This becomes the *h*-BaO_3 layer in the hexagonal phase. This twinning produces two non-equivalent Ba and Fe/W cations. The Fe_2–Fe_2 separation is clearly influenced by the concentration of O_1 site vacancies in the layer separating the Fe_2 atoms. This separation increases with increasing O_1 vacancy concentration as a result of greater Coulomb repulsive forces between Fe cations within the face-sharing octahedra. To reduce the repulsion, the oxygens move closer together distorting the octahedron itself.

In the cubic structure (see Fig. 8a), the (111) planes are close-packed; each Ba atom in a (111) plane is surrounded by six oxygen atoms and forms a BaO_3 plane. Along the

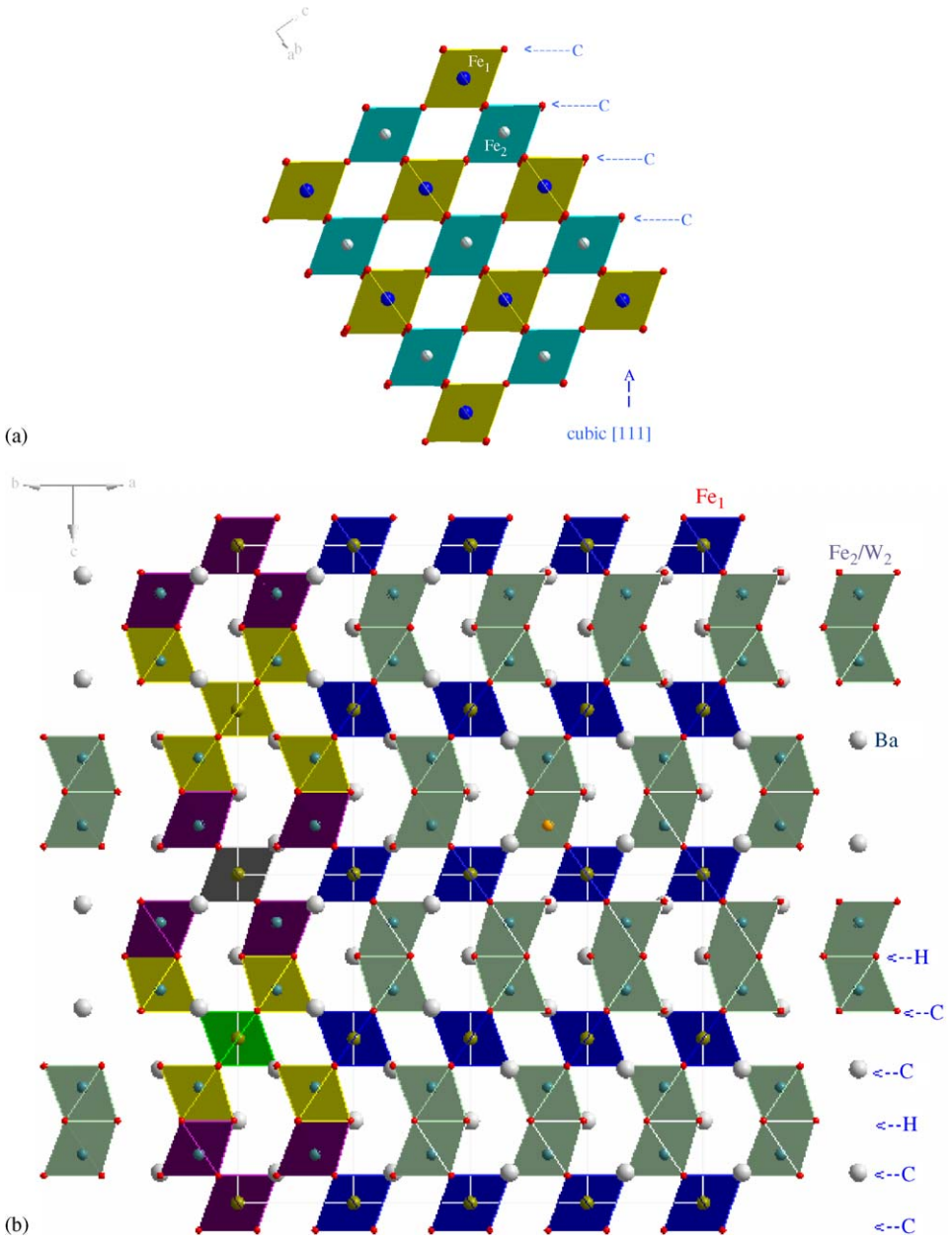

Fig. 8. Projections along [101] of the octahedral arrangements in the $Ba_3Fe_2WO_{9-\delta}$: (a) cubic structure and (b) hexagonal structure. *c* and *h* denote corner-sharing and face-sharing of Fe/W octahedra.

[111] direction, the Ba–O_3 planes stack on each other at a distance of $a/\sqrt{3}$ translated with respect to each other by the 1/3 [112] translation vector. Thus the stacking sequence in the [111] direction shows the three-layer periodicity of *ccc*. The structure of hexagonal BFWO is closely related to the cubic perovskite structure. The difference between these structures is in their modes of the stacking of layers consisting of BaO_3 planes.

The unit cell volume (referred to a primitive perovskite cell) is significantly larger for the hexagonal $P6_3/mmc$ structure in comparison with the cubic $Fm-3m$ one (67.5 and 66.7 $Å^3$, respectively, at room temperature). This expansion originates from the repulsion of Fe^{3+} in the face-sharing double octahedras in the hexagonal layers.

Using the tolerance factor, *t*, which is an expression for the mismatch between equilibrium A–O and B–O bond lengths in perovskite structure, the phase transformation from the hexagonal structure to the cubic one in BFWO corresponds to a decrease of the *t* parameter, which is equal to 1.03 for $Ba_3Fe_2WO_9$ and to 1.004 for $Ba_3Fe_2WO_{8.45}$.

This hexagonal → cubic phase transformation is not unique. Several authors indicate that this hexagonal perovskite polytype can be transformed to a cubic perovskite structure by cationic substitution and/or the application of pressure [25,26]. The same phase transformation accompanying an increase in oxygen deficiency was reported for the $SrMnO_{3-\delta}$ [23] and $(Sr,Ca)MnO_{3-\delta}$ [27] perovskites. It was suggested that the initial hexagonal

structure remains stable up to the maximum oxygen content, which should be near $SrMnO_{2.75}$.

It can be noted that there is an opposite cubic–hexagonal phase transformation in perovskites. It was shown in [28] that the hexagonal perovskite structure could be generated from cubic $BaTiO_3$ by partial substitution of the Ti cations with other transition metal atoms (M), to give the formula unit $Ba_3Ti_2MO_9$. More recently it was discovered in [29] that the small fractional substitution of Mn in $Ba(Ti_{0.98}Mn_{0.02})O_3$ stabilizes the hexagonal phase which exist for pure $BaTiO_3$ above 1460 °C [30].

There are mainly three factors responsible for the change of magnetic order in perovskites. The first is the change in the Fe–O bond distance, the second is the Fe–O–Fe bond angle, and the third is the number of nearest neighbours. In the case of BFWO the increase in the oxygen vacancy concentration leads to remarkable changes of all indicated factors that can have an effect on magnetic ordering. In complex perovskites $A_2B\,B'O_6$ involving diamagnetic B′ cations (W in our case) arranged in alternate octahedral sites, there are two competing interactions between magnetic B cations (Fe for our composition); a 180° B–O–B′–O–B σ superexhange and a 90° B–O–O–B π superexchange. Very often an antiferromagnetic coupling via π superexchange mechanism is predominant in these complex oxides [31].

For a cubic lattice where (4a) positions are fully occupied by Fe cations, and (4b) sites are statistically occupied by 0.33 Fe, the long-range magnetic connections via Fe_{4a}–O–Fe_{4b}–O–Fe_{4a} paths may originate because following [32] only 9% of Fe_{4a} cations are not connected to at least one of the Fe_{4b} cations. The perfect ferromagnetic coupling between up Fe spins at (4a) sites and down Fe spins at (4b) positions would ideally give a net magnetization about 3.33 μ_B, but this would realize only in the case of perfect coherence between neighbouring paths. The maximum magnetization registered at 10 K for non-stoichiometric BFWO is smaller than the predicted value, that probably arising from some part of non-connected Fe cations.

The hexagonal structure of BFWO consists of dimers of face-sharing octahedra separated by single corner sharing octahedra (see Fig. 5b). From this figure it is clear that there are two distinct sites for Fe cations: Fe_1 shares only vertices with adjacent octahedra whilst Fe_2 shares both vertices and faces with neighbouring octahedra. Two kinds of the magnetic interactions are important for determining magnetic properties of hexagonal BFWO. One is the magnetic interaction between two Fe cations in Fe_2O_9 dimers; this brings about a strong antiferromagnetic coupling. Another important interaction is the one between two different Fe_1 and Fe_2 cations in this kind of structure via the linear Fe_1–O–Fe_2 pathway, which is in common with the case of double perovskites. This different geometry (the face-sharing and corner-sharing octahedra) and a variable degree of oxygen content can lead to dramatic differences in superexchange interactions compared with an apex-shared connectivity in the cubic structure, which adopted the 180° Fe–O–Fe angle [33].

It is important to note that we also tried to prepare other BFWO samples with oxygen content between 8.45 and 9.0. We were able to obtain only one new additional compound with composition $Ba_3Fe_2WO_{8.72(2)}$, which also showed up to be a cubic perovskite (space group $Fm-3m$, $a = 8.098(1)$ Å).The results of magnetic measurements (see Figs. 1 and 2) suggest the material is in fact ferrimagnetic below 340 K as in the case $Ba_3Fe_2WO_{8.45}$.

5. Concluding remarks

In summary, we have presented a detailed crystallographic characterization of different BFWO phases. Magnetic measurements, together with X-ray and neutron diffraction have been carried out in the temperature range 10–700 K to study the structure and physical properties of $Ba_3Fe_2WO_{9-\delta}$ prepared by varying heat treatments in different environments.

It was shown that at room temperature the stoichiometric single-phase compound ($\delta = 0.00$) crystallizes in a hexagonal 6H-perovskite structure (space group $P6_3/mmc$). The hexagonal samples, heat-treated in argon gas, show some amount of oxygen vacancies causing a transformation to an oxygen-deficient phase ($\delta = 0.55$), which is an ordered cubic perovskite structure (space group $Fm-3m$). Through NPD and magnetic susceptibility measurements, the ferrimagnetic ordering temperature was estimated to be about 340 K. Phase relations, crystal and magnetic structure of a new non-stoichiometric phase were described. It was shown that a relatively small concentration of oxygen vacancies is effective for controlling the crystal and magnetic structure and fundamental physical properties of this perovskite. The oxygen deficiency implies a partial reduction of the Fe sublattice and therefore a change of magnetic properties. An oxygen non-stoichiometry tends to stabilize the long-range magnetic order and to increase the temperature of magnetic phase transition.

The change of magnetic ordering observed for both the hexagonal and cubic structures are explained on the basis of obtained crystallochemical data (Fe–O bond distance, Fe–O–Fe bond angle and the number of nearest neighbour ions). Finally, this study principally underlines the importance of slight oxygen non-stoichiometry as an effective parameter for the preparation of new complex metal oxides with a perovskite structure having the specified structural and magnetic properties.

Acknowledgments

The present work has been supported by the Royal Swedish Academy of Sciences and the Swedish Strategic Foundation (SSF), within the frames of the program ‘‘Complex oxides for advanced applications’’, which is gratefully acknowledged.

References

[1] T. Kimura, T. Goto, H. Shintani, K. Ishizaka, T. Arima, Y. Tokura, Nature 426 (2003) 55.
[2] T. Goto, T. Kimura, G. Lawes, A.P. Ramirez, Y. Tokura, Phys. Rev. Lett. 92 (2004) 257201.
[3] N. Hur, S. Park, P.A. Sharma, J.S. Ahn, S. Guha, S.W. Cheong, Nature 429 (2004) 392.
[4] C. Ederer, N.A. Spaldin, Nature 431 (2004) 849.
[5] N.A. Hill, Annu. Rev. Mater. Res. 32 (2002) 1.
[6] N.A. Hill, J. Chem. Phys. B 104 (2000) 6694.
[7] G.A. Smolensky, I.E. Chupis, Sov. Phys.-Uspekhi 25 (1982) 475.
[8] G. Blasse, J. Inorg. Nucl. Chem. 27 (1965) 993.
[9] Yu.N. Venevtsev, V.V. Gagulin, Ferroelectrics 162 (1994) 23.
[10] Y.N. Venevtsev, E.D. Politova, S.A. Ivanov, Ferro- and Antiferroelectrics of Barium Titanate Family, Chemistry, Moscow, 1985.
[11] S.A. Ivanov, S.G. Eriksson, R. Tellgren, H. Rundlof, Mater. Res. Bull. 36 (2001) 2585.
[12] S.A. Ivanov, S.G. Eriksson, R. Tellgren, H. Rundlof, Mater. Res. Bull. 39 (2004) 615.
[13] S.A. Ivanov, S.G. Eriksson, R. Tellgren, H. Rundlof, Mater. Res. Bull. 39 (2004) 2317.
[14] L. Katz, R. Ward, J. Inorg. Chem. 3 (1964) 205.
[15] G. Blasse, Philips Res. Rep. 20 (1965) 327.
[16] V.V. Gagulin, N.V. Fadeeva, A.G. Belous, Phys. Status Solidi (A) 48 (1978) 183.
[17] D.B. Harari, These de doctorat d′Etat, Orsay, 1975.
[18] G. Matzen, P. Poix, J. Solid State Chem. 33 (1980) 341.
[19] J. Rodriguez-Carvajal, Physica B 192 (1993) 55.
[20] R.D. Shannon, Acta Crystallogr. (A) 32 (1976) 751.
[21] I.D. Brown, in: M.O. Keefe, A. Navrotsky (Eds.), Structure and Bonding in Crystals, vol. 2, Academic Press, New York, p. 1.
[22] L. Katz, R. Ward, Inorg. Chem. 3 (1964) 205.
[23] T. Negas, R. Roth, J. Solid State Chem. 1 (1970) 409.
[24] Y.C. Wu, H.Y. Lu, Philos. Mag. 84 (2004) 3467.
[25] J.M. Longo, J.A. Kafalas, Mater. Res. Bull. 3 (1968) 687.
[26] P.D. Battle, C.W. Jones, P. Lightfoot, R. Strange, J. Solid State Chem. 85 (1990) 144.
[27] J. Topfer, U. Pippardt, I. Voigt, R. Kriegel, Solid State Sci. 6 (2004) 647.
[28] J.G. Dickson, L. Kartz, R. Ward, J. Amer. Chem. Soc. 83 (1961) 3026.
[29] F. Ren, S. Ishida, S. Mineta, J. Ceram. Soc. Japan 102 (1994) 105.
[30] K.W. Kirby, B.A. Wechsler, J. Am. Ceram. Soc. 74 (1991) 1841.
[31] S.H. Byeon, S.S. Lee, J.B. Parise, P.M. Woodward, N.H. Hur, Chem. Mater. 17 (2005) 3552.
[32] R.M. Pinacca, M.C. Viola, J.A. Alonso, J.C. Pedregosa, R.E. Carbonio, J. Mater. Chem. 15 (2005) 4648.
[33] J.B. Goodenough, Magnetism and Chemical Bond, Wiley, New York, 1963.